Noname manuscript No.
(will be inserted by the editor)

Hybrid potential field based control of differential drive mobile robots

Luis Valbuena · Herbert G. Tanner

Received: date / Accepted: date

Abstract This paper suggests a new way for nonholonomic mobile robots to navigate in obstacle environments using potential fields based on navigation functions. The proposed strategy is a time-invariant feedback control design with the distinguishing feature that it requires almost no switching compared to alternative methodologies of the same nature. Asymptotic convergence with collision avoidance for the proposed approach is established analytically, and the method is demonstrated on a differential-drive skid steering mobile robot.

Keywords Obstacle avoidance · potential fields · nonholonomic systems

1 Introduction

This paper presents a methodology for navigation of wheeled mobile robots in planar environments with obstacles, using reference vector fields which are functions of position. The reference vector fields are derived originally as potential fields of navigation functions defined on the robot position, and then transformed locally around the destination configuration to enable the simultaneous regulation of both position and orientation.

1.1 Background

The paper focuses on the problem of nonholonomic robot posture control in the presence of *obstacles*. For this reason, a detailed description of the extensive literature on unconstrained nonholonomic stabilization is not attempted. Part of the reason why unconstrained approaches cannot be applied directly in environments with obstacles is that a large portion of them employ state transformations; the impact of such transformations on the free workspace

Department of Mechanical Engineering, University of Delaware, Newark, DE, USA E-mail: {valbuena, btanner}@udel.edu

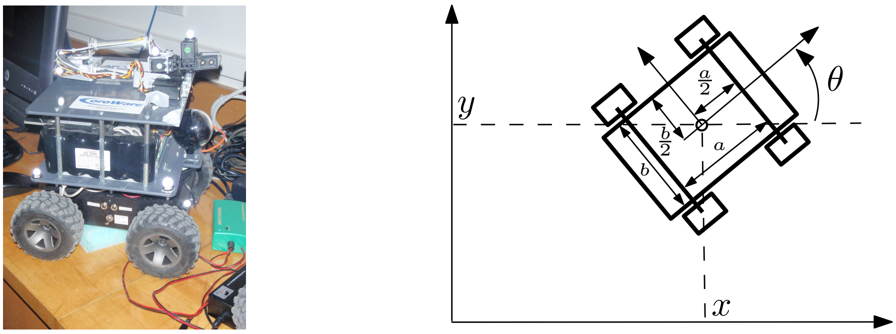

(a) The mobile robot. (b) The robot's abstraction.

Fig. 1 The mobile robot for which the proposed approach is developed. This platform uses a four-wheel-drive skid steering mechanism to maneuver, it accepts linear and angular velocity commands, and its lightweight construction (6.5 kg) allows a reasonable kinematic modeling in the form of the equations of a unicycle.

is unclear. And while it is known that local nonholonomic motion planners which satisfy a certain topological property [46] can approximate segments of a holonomic collision free path with feasible ones, the variable utilization of feedback in existing nonholonomic planners can limit their effectiveness since models and measurements are rarely perfectly accurate. In this paper, therefore, the goal is to attack the problem without decomposing it into separate planning and control phases, and be able to utilize state feedback continuously, throughout the duration of the motion, without switching between different control regimes.

One way of using feedback in robot motion planning is by means of potential fields. Using potential fields for robot navigation has a long history, and [7] offers an introduction and some historical perspective. Reference [20] is one of the first appearances of the method in literature. One important problem with potential field implementations is the appearance of local minima; these are attractive configurations where the field is singular and the robot gets "trapped." Navigation functions are introduced in [22,42] as a solution to the problem of local minima. In the navigation function approach, these undesirable attractors can be transformed into saddle points that have regions of attraction of measure zero. Applying potential fields to systems with nonholonomic constraints, however, is nontrivial because the potential field direction can fall into the subspace of velocity vectors which are infeasible for the system. In any case, it is known that there can be no continuous static state feedback controllers that can stabilize a nonholonomic wheeled mobile robot to some point [4].

Between the well researched areas of nonholonomic control design for systems without drift [1,3,12,27,37,41,44,53], and motion planning using potential fields [2,10,21,24,42,47], the area is not so well explored. The solutions we find may be broadly categorized in three or four groups, and there are a handful of elements in each group.

One general approach is to start with a given collision free path and modify it [28, 45, 46] or approximate it [29] with local trajectories that satisfy the robot's nonholonomic constraints. Another is to use a navigation function of the robot's position and include an artificial obstacle; in one implementation of such an obstacle is a "cup-shaped" barrier around the goal position, forcing the mobile robot to approach the target from a single direction and with orientation of zero or π [25]; in another implementation, this obstacle is of measure zero, it includes the destination configuration and is aligned with the direction along which the nonholonomic constraint prevents the robot to move when it is at the destination [43, 48–50]. A third approach uses a navigation function defined on the full configuration space of the system. A hybrid or switching strategy can then be used. In [48, 49] switching strategies are used, while [51] uses time-varying inputs designed to push the system away from configurations where the system vector field becomes orthogonal to that of the navigation function gradient. In another switching approach the robot is steered either along directions that decrease the function, or along the boundary of the function's level set until a new direction of decrease can be found [33, 34]; a similar switching strategy is explored in [32] for holonomic systems moving in uncertain environments. In a recent approach [18], cell decomposition methods are combined with navigation functions in the spirit of [9], but in a way that it can be applied to systems with nonholonomic constraints.

Such solutions to the problem of nonholonomic navigation in obstacle environments using static state feedback may be algorithmically complete but there are always limitations. In the case where holonomic collision-free paths are modified, the required trajectory optimization or the alternative use of time-varying inputs can take a toll on convergence time and may yield erratic convergence.[1] In addition, real-time replanning may be problematic, and the existence of uncertainty in both robot and environment models necessitates the use of feedback throughout the whole duration of the maneuver. If time-varying control is not employed, Brockett's condition [5] necessitates switching. When switching is employed [33], control discontinuities may provide faster convergence but *cannot overcome* the limitations of Brockett's necessary condition, and thus the attractive equilibria are not stable in the sense of Lyapunov.[2] Control discontinuities do not automatically lift the limitation set by Brockett's necessary condition for stabilization.[3]

[1] See [38] for an insightful discussion on the performance of time-varying nonholonomic stabilizing controllers.

[2] In fact, it has been shown [11] that systems affine in control, stabilizable using discontinuous feedback with solutions defined in the sense of Filippov [15], can also be stabilized using *continuous time-invariant feedback.*

[3] It is known however, that in the case of sampled-data (piecewise constant) control inputs, the existence of a control law that asymptotically brings the state to zero implies the existence of a locally bounded feedback stabilizer [8].

In the approaches that use dipolar fields, the limitation that stems from Brockett's condition still applies, and insisting on establishing asymptotic stability requires a slightly different definition of stability compared to the one in the sense of Lyapunov (see [26], for example). Practically, regions around the equilibrium where initial conditions are selected and trajectories confined in, cannot be balls; they have to be some differently shaped *neighborhoods*. Nevertheless, the control strategy that hinges on dipolar fields requires less frequent switching, and the latter occurs mainly at the boundary of the obstacle-free workspace. The downside is that with the introduction of the artificial obstacle, the workspace is partitioned in two invariant regions, and the robot is not capable of crossing that boundary. Finally, in [18], the orientation of the robot is not stabilized, as in the case of [35]. In the latter, a holonomic potential field is projected on the vehicle's feasible directions of motion; when the desired direction is in the null space of the Pfaffian constraint matrix, however, no feasible direction for the vehicle can be found.

There is a significant body of work on potential field based control of nonholonomic systems which does not directly relate to the problem addressed here. One such example is that of trajectory tracking in the presence of obstacles [23,30], which is however a different problem than that of posture control, and Brockett's condition does not necessarily apply. There are also hierarchical potential field approaches [40] in which a high level planner designs a collision free path and a local potential field keeps the robot inside a "bubble" along this path; the hierarchical decomposition circumvents some technical difficulties but makes the closed loop system susceptible to model and environmental uncertainty, just like the approach that approximates holonomic path solutions. The existing work on harmonic potential fields, on the other hand [14, 16, 17, 36, 52], whether with switching, sliding-mode, or other controllers, focuses on position stabilization and do not attempt to stabilize the final orientation of the vehicle.

1.2 Contributions

The approach of this paper attempts to alleviate some of the problems encountered when trying to navigate nonholonomic mobile robots in cluttered environments. Specifically, the proposed method

- ensures collision avoidance without affecting the connectivity of the free space (cf. [43, 48]);
- offers analytic proofs for the (almost) global attractive properties for the destination configuration, both in terms of position and orientation (cf. [18]);
- allows the use of potential fields that do not include the vehicle's orientation, and
- does not involve on-line control switching (cf. [33]).

The latter is the main technical novelty of the proposed method.

Not surprisingly, the methodology comes with limitations of its own. In its current form, the algorithm applies to planar systems (unicycles), although our ongoing work [39] shows promise for the ability to generalize to more dimensions. Second, the closed-loop trajectories generated are not optimal, neither with respect to time nor in terms of path length. Finally, the approach is based on the hypothesis that the robot can perform arbitrarily tight turns while translating, although it is not allowed to turn in place.

1.3 Organization and overview

The basic idea behind the proposed method is to first steer the mobile robot in a neighborhood of its desired *position*, using a potential field generated by a navigation function defined on the robot's position only. To do so, a feedback controller aligns the robot's velocity with that of the potential field, and keeps the robot moving along the field direction. Close to the desired position, the potential field is locally transformed: its vectors are rotated by an angle that depends on the position around the destination so that the resulting field takes the form of that of a magnetic dipole, with a moment aligned to the robot's desired orientation. The same motion controller then makes the robot approach its destination along the direction of that moment. In this way, the position of the robot is directly controlled, while the orientation is regulated implicitly via the shape of the flow lines of the field around the destination. The important difference compared to existing dipolar field methods is that the topology of the workspace is not affected by the introduction of some artificial obstacle.

Cases where position and orientation of a mobile robot need to converge concurrently (rather than the robot turning in place at the desired position) are found in applications where that same robot serves as a formation leader, or when it is attached to a trailer the kinematics of which should not be included in the systems equations. Another example is found in problems of path following or waypoint navigation, where intermediate waypoints are also associated with path tangency (orientation) specifications.

A formal statement of the problem addressed is found in Section 2. Sections 3 and 4 contain the main technical results and document the construction of the reference field for the robot and its useful properties (Section 3), as well as the feedback controller with its convergence properties (Section 4). Simulation results that corroborate the theoretical convergence predictions are provided in Section 5. Section 6 describes an experimental implementation of the proposed method on a differential-drive robot. Finally, Section 7 concludes the paper with a summary of the contributions and a brief discussion on possible extensions.

2 Problem Statement

The kinematics of the skid-steering mobile robot of Figure 1 can be reasonably captured by the equations of the unicycle:

$$\dot{x} = v \ \cos\theta \tag{1a}$$

$$\dot{y} = v \ \sin\theta \tag{1b}$$

$$\dot{\theta} = \omega \ , \tag{1c}$$

where x and y represent the position of the unicycle on the plane and θ its orientation, measured with respect to the x-axis. The variables v and ω are the control inputs: translational and rotational speed, respectively. Although arbitrarily small curvature radii can be achieved, the robot is not supposed to be able to turn in place.

Let $q \triangleq (x, y)^\mathsf{T}$, where $^\mathsf{T}$ denotes transpose. Assume that $q \in \mathcal{W}$, where $\mathcal{W}$ is the planar workspace of the robot, mathematically described as a closed ball in $\mathbb{R}^2$ containing the origin. Note that any star-shaped region can be diffeomorphically transformed into a sphere [42]. For this same reason, we assume the obstacles in the robot's workspace to be ultimately represented by spheres, $\mathcal{O}_i \in \mathcal{W}$, for $i \in \{1, \ldots, m\}$. These spheres are isolated, that is $\mathcal{O}_i \cap \mathcal{O}_j = \emptyset$ for every $i \neq j$ with $i, j \in \{0, \ldots, m\}$. The workspace boundary is an obstacle, expressed as the complement of $\mathcal{W}$ in $\mathbb{R}^2$: $\mathcal{O}_0 \triangleq \mathbb{R}^2 \setminus \mathcal{W}$.

The problem is to design time-invariant, feedback control laws $v = v(x, y, \theta)$ and $\omega = \omega(x, y, \theta)$ such that (1) converges asymptotically to $(x, y, \theta) = (0, 0, 0)$ from almost all (with the possible exception of a set of measure zero) initial configurations $\big(x(0), y(0), \theta(0)\big)$, while satisfying $q(t) \neq \mathcal{O}_i$, for all $i \in \{0, \ldots, m\}$, and for all $t > 0$.

3 Reference Vector Field

Let ∂S denote the boundary of a domain $S \subset \mathbb{R}^n$ and assume the existence of radially unbounded functions $\beta_i(q)$, with $i \in \{0, \ldots, m\}$ such that

1. $\beta_i(q) = 0$ if $q \in \partial\mathcal{O}_i$
2. $\beta_i(q) < 0$ if $q \in \mathcal{O}_i$
3. $\beta_i(q) > 0$ if $q \neq \mathcal{O}_i \cup \partial\mathcal{O}_i$.

For the case where $\mathcal{O}_i$ have spherical boundaries, as considered in this section, the functions β_i can be simply expressed as $\|q - q_i\|^2 - {r_i}^2$, where q_i is the center of $\mathcal{O}_i$ and r_i its radius for $i \in \{1, \ldots, m\}$. For $i = 0$, let $\beta_0 \triangleq {r_0}^2 - q^2$. Also let $\gamma(q) \triangleq \|q\|^2$. Then it is known [22] that the function

$$\varphi(q) = \frac{\gamma}{\left[\gamma^\kappa + \prod_{i=0}^m \beta_i(q)\right]^{\frac{1}{\kappa}}} \tag{2}$$

is a navigation function on $\mathcal{W} \setminus \bigcup_{i=1}^m \mathcal{O}_i$ if a sufficiently large value of parameter κ is selected. This means that the vector field defined by the negated gradient,

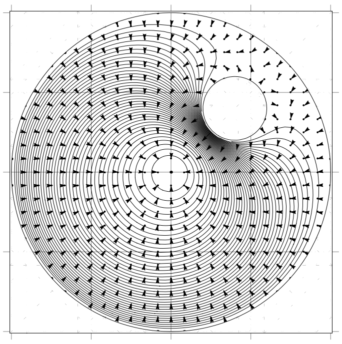

Fig. 2 An example of the classical sphere-world navigation function construction. The negated gradient of the navigation function is shown superimposed on its contour plot. It can be seen that the field points away from the spherical obstacle and toward the origin, which is the destination point.

$-\nabla_q\varphi(q)$, can be adjusted so that its integral curves converge to $q = 0$ from almost all initial conditions in $\mathcal{W}\backslash\bigcup_{i=1}^{m}\mathcal{O}_i$ (Fig. 2). The only initial conditions from which these trajectories do not converge form a positively invariant set of measure zero, consisted of isolated components each including an unstable equilibrium coinciding with a saddle of $\varphi(q)$. There are m such unstable equilibria. Define the discontinuous map $\varGamma$ which in local coordinates is expressed as a matrix

$$\varGamma(z) = \begin{bmatrix} -\cos z & \sin z \\ -\sin z & -\cos z \end{bmatrix} \ , \tag{3}$$

where $z \triangleq s_d(x, y; a) \arctan2(y, x) + \pi \operatorname{sign}(y)\big(1 - s_d(x, y; a)\big)$ and

$$s_d(x, y; a) = \exp\left(-\frac{a}{(1 - \varphi(x, y))^2} + a\right) \ , \tag{4}$$

in which $0 < a < 1$. Despite being discontinuous, $\varGamma$ is nonsingular everywhere. Function s_d plays the role of a "switch" (as in [42]) turning different components of the argument z in $\varGamma$ on and off. The same notation is used here as in the *analytic switch* functions of [42], although s_d is not analytic everywhere in $\mathbb{R}^2$; it fails to be so on $\partial\bigcup_{i=1}^{m}\mathcal{O}_i$.

What $\varGamma$ basically does is to rotate a vector at a given point (x, y) by an angle equal to the vector from the origin to (x, y). When applied to the planar vector field with the structure of an asymptotically stable proper node, $\varGamma$ makes it resemble the field of a point dipole (Figure 3). The idea behind this construction is that if a system is made to track the flow lines of the transformed field, it reaches the origin with an orientation angle converging to zero, without the orientation being directly regulated.

When the transformation is applied, it generates a bounded segment of the positive horizontal semi-axis starting at the origin, from which the reference vector field diverges. At the end point of this segment, the one closer to the origin, a discontinuity point in the vector field appears: since the transformation is nonsingular, and the potential field of the navigation function vanishes

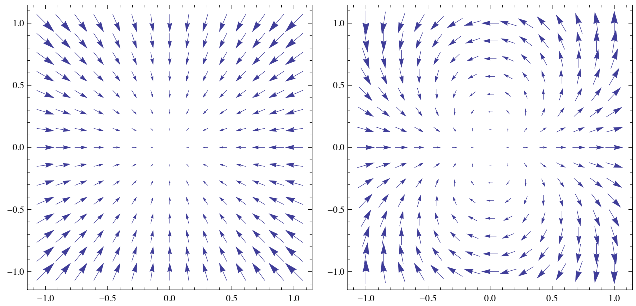

(a) Stable proper node. (b) Rotated field via Γ.

Fig. 3 The effect of Γ on a convergent vector field. The field in 3(b) was produced by mapping the field in 3(a) through a map Γ in which s_d was set identically to one.

nowhere but at given isolated saddle points, there has to be a point where the transformed field reverses direction *without vanishing*. In fact, the vector field becomes nonsmooth along the $y = 0$ line, and an unstable nonsmooth equilibrium appears (see Lemma 3 in Appendix A).

Several interesting properties can be shown for the transformed field. Each one of them is established analytically as a lemma in Appendix A.

1. All integral curves of the transformed field contain the origin, and the origin is the only singular point of the vector field.
2. The transformed field points away from obstacle regions.
3. All stationary points of the transformed field other than the origin have attraction regions of measure zero.
4. All integral curves of the transformed field converge to the origin asymptotically along the negative x axis, and their common derivative at $q = 0$ is aligned with the x axis.

The following section exploits these properties to design feedback control laws with collision avoidance and (almost) global convergence properties for both position and orientation.

4 Navigation Strategy

The objective of the control law is to align the system's vector field with the reference field. One solution may be[4]

$$v = k_1 \tanh(\|q\|) \tag{5a}$$

$$\omega = -k_2 \left[\theta - \arctan 2\left(f_y, f_x\right)\right] + \frac{v}{\|F\|^2}\left(f_x\left(\frac{\partial f_y}{\partial y}\sin\theta + \frac{\partial f_y}{\partial x}\cos\theta\right) - f_y\left(\frac{\partial f_x}{\partial y}\sin\theta + \frac{\partial f_x}{\partial x}\cos\theta\right)\right) \tag{5b}$$

[4] After its introduction in [48], this controller has been frequently adopted and used in different versions [6, 13, 31].

where $k_1 > 0$ and $k_2 > 0$ are constant control gains, and $(f_x, f_y)^\mathsf{T} \triangleq F = \Gamma \nabla \varphi(x, y)$. Intuitively, a good choice of control gains is one that enables the orientation kinematics (5b) to converge considerably faster compared to the longitudinal kinematics (5a).

Proposition 1 *Control law* (5) *makes* (1) *converge to an arbitrarily small neighborhood of* $x = y = \theta = 0$ *asymptotically from almost all initial conditions in* $\mathcal{W} \setminus \bigcup_{i=1}^{m} \mathcal{O}_i$.

Proof The purpose of (5b) is to align the direction (1) to the direction of the transformed vector field, $\theta_d \triangleq \arctan 2\,(f_y, f_x)$ exponentially; the last term in (5b) is the rotational velocity feedforward, designed to bring the closed loop dynamics of θ to the form $\dot{\theta} - \dot{\theta}_d = -k_2(\theta - \theta_d)$. As $(\dot{x}, \dot{y})$ becomes parallel (forming a positive inner product) to F exponentially fast, the dynamics of the closed loop system can be thought of as made up of two systems with different time scales. The fast dynamics of $\theta - \theta_d$ converge exponentially fast to zero. Taking $\varepsilon = \frac{k_1}{k_2}$, we see that the resulting quasi steady state is uniquely determined as $\theta = \theta_d$, and the reduced (slow) dynamics of (x, y) have the form:

$$\begin{aligned} \dot{x} &= \alpha(q) f_x \\ \dot{y} &= \alpha(q) f_y, \end{aligned}$$

where $\alpha(q)$ is a positive definite function (a scaling factor relating $\|F\|$ to $k_1 \tanh(\|q\|)$). A singular perturbation argument [19, Theorem 11.1] then ensures that for a small enough ε, the closed loop trajectories $(x(t), y(t))$ will be close to some integral curve of F by $O(\varepsilon)$. As Lemma 4 (in Appendix A) suggests, F converges to $(0, 0)$ following the negative x axis asymptotically.

In the case of a linear velocity v with constant sign, and in practical implementations, caution needs to be exercised so that the system does not "overshoot." If the system crosses the y axis on its approach to the origin, the reference field will then push it away along a big circle that loops back. In theory, this does not happen because $(x(t), y(t)) \to (0, 0) \Rightarrow v \to 0$, so that the system appears to land gently at the origin. In the remaining of the section we address precisely this issue, by allowing the inversion of the sign of v when the y axis is crossed on the approach phase. The switching is done locally around $(0, 0)$, so as not to interfere with collision avoidance.

Remark 1 Even when a local sign switching strategy for v is adopted, the point $(0, 0, 0) \in \mathsf{SE}(2)$ is still *not* an asymptotically stable equilibrium for $-\Gamma \nabla \varphi$ in the sense of Lyapunov. One can fairly easily establish asymptotic convergence in the same lines as in Proposition 1, but Lyapunov stability essentially requires that for sufficiently small perturbations of the initial conditions around the origin, the trajectories can be contained in an arbitrarily small ball. In this case, perturbations along the y-axis require the trajectory to make a "full circle" before returning to the equilibrium; the orientation of the unicycle needs to change dramatically, irrespectively of whether it goes forward or backward.

This is why in the proof of Proposition 1 we use a singular perturbation argument only to show that the closed loop trajectories will be ϵ-close to the integral manifolds of the reference field.

No optimality is claimed for the trajectories of the closed loop system under (5), neither with respect to time, nor with respect to path length. (Note that similar issues arise, and are discussed in [33].) The goal of this paper is different: to offer a way of achieving asymptotic convergence and collision avoidance for nonholonomic systems while *reducing switching*. More efficient strategies can be employed if switching can be tolerated, but chattering behavior is likely to be an issue in implementation.

The following alternative control law utilizes switching but implements it in a way that it can only occur locally around the destination. It eliminates the need to perform extensive maneuvering to return to the equilibrium if the vehicle crosses the y axis while close to its desired position. This strategy induces *hybrid* dynamics for the system, in which the vehicle can reverse its speed as a means of reaching its destination along a shorter path, if certain logic (guard) conditions are satisfied.

Let us first specify the initial condition for (1) explicitly as $\xi = (x_0, y_0, \theta_0)$, and modify the navigation strategy of (5) as follows:

$$v = k_1 \operatorname{sign}\big(\varepsilon - x_0 \; s_d(x_0, y_0; a')\big) \tanh\left(\sqrt{x^2 + y^2}\right) \tag{6a}$$

$$\omega = -k_2 \left[\theta - \operatorname{arctan2}\,(f_y, f_x)\right] + \frac{v}{\|F\|^2}\left(f_x\left(\frac{\partial f_y}{\partial y}\sin\theta + \frac{\partial f_y}{\partial x}\cos\theta\right) - f_y\left(\frac{\partial f_x}{\partial y}\sin\theta + \frac{\partial f_x}{\partial x}\cos\theta\right)\right), \tag{6b}$$

where $\varepsilon > 0$ is a small constant, and $a' >> a$. Then the overall closed-loop system behavior can then be captured by the following hybrid system description.

Definition 1 The closed loop dynamics of (1) are given in the form of a hybrid system $\mathbf{H}$ which is a tuple $\mathbf{H} = (\mathcal{X}, \mathcal{K}, F_k, \mathcal{X}_0, \mathcal{G})$ consisting of:

- $\mathcal{X} = (\mathcal{W} \setminus \bigcup_{i=1}^{m} \mathcal{O}) \times \mathbb{S}^1$ is the continuous state space of the system with $(x, y, \theta) \in \mathcal{X}$ being the state;
- $\mathcal{K} = \{1\}$ is a (trivial) set of discrete system modes indexing different continuous component dynamics;
- $F_k : \mathcal{X} \to T\mathcal{X}$, for $k \in \mathcal{K}$ is a collection of closed-loop continuous vector fields, given by (1) and (6);
- $\mathcal{X}_0 \subseteq \mathcal{X}$ is the set of possible initial conditions for the system's continuous state, based on which the integral curves of F_k are defined as $\Phi_k(t;\xi)$, with $\xi \in \mathcal{X}$, $\Phi_k(0;\xi) = \xi$ and $\frac{d}{dt}\Phi_k(t;\xi) = F_k(\Phi_k(t;\xi))$;
- $\mathcal{G}$ is the guard condition that enables a discrete reset in $\mathcal{X}_0$:

$$\mathcal{G} = \{\varepsilon - x(t-\delta)\; s_d(x(t-\delta), y(t-\delta); a') < \varepsilon \text{ and } (\forall\, \tau \in (t-\delta, t])[\varepsilon - x(\tau)\; s_d(x(\tau), y(\tau); a') > \varepsilon] \text{ and } v > 0\}\ ,$$

  for a small $\delta > 0$;

– $S : \mathcal{X}_0 \to \mathcal{X}_0$ is the reset function for $\xi \in \mathcal{X}_0$, according to which $\xi := \big(x(t), y(t), \theta(t)\big)$.

Based on the hybrid dynamics of Definition 1, (1) first chooses the sign of its translational speed based on its initial condition; it goes on reverse only if it is in an obstacle free neighborhood of the origin, on the right of the y axis. This neighborhood is specified by the predicate $\varepsilon - xs_d(x, y; a') < 0$. If it finds itself inside that neighborhood for a time period larger than δ seconds and still has a positive speed, then it switches to negative speed, and while still aligned to the reference vector field, it approaches the destination in reverse. The time delay of δ seconds is introduced in order to alleviate possible chattering phenomena. In this way, if the unicycle "overshoots" as it approaches the destination, it does not turn around making a full circle before it converges again. The steady state behavior under (6) as implemented in the hybrid system of Definition 1 is practically that of the two-dimensional, single-input system in [26] $\dot{x} = (x^2 - y^2)u$, $\dot{y} = 2xy\,u$, which consists of going in reverse ($u < 0$) along the circular arcs tangent to the origin if initialized to the right of the y axis, and going forward ($u > 0$) along the arcs if initialized on the left. Given the results of [26], and with Proposition 1 ensuring the convergence of the trajectories of the closed loop unicycle on the integral curves of F, a detailed analytical derivation of the asymptotic convergence for (1) under (6) is superfluous.

5 Numerical Results

We create a simple two-dimensional sphere world workspace, centered at the origin, with a boundary of radius $r_0 = 1$ m and a single obstacle with radius $r_1 = \sqrt{0.2}$ m centered at $(0.4, 0.4)$ m. The destination configuration is set at the origin $q_d = (0, 0)$ m. A navigation function of the form (2) is built on this workspace and its parameter is set to $\kappa = 2$, yielding a virtual landscape the contours of which are shown in Figure 4. The unicycle is initiated at configuration $x(0) = 0.5$ m, $y(0) = 0.7$ m and $\theta(0) = -\frac{\pi}{2}$, on the side of the obstacle not facing the destination. We assume knowledge of the position and orientation variables (x, y, θ) of the unicycle, which are used as feedback. The collision-avoidance maneuver of the unicycle under (5), and its path to the destination is shown in Figure 4, while Figure 5 depicts the time history of the three configuration variables (x, y, θ) indicating that all three of the configuration variables converge.

With regards to the path shown in Figure 4, a few comments are in order. It can be argued that a faster, or shorter, path could have been followed to the destination, which motivates the use of the hybrid navigation strategy described in Definition 1. With this strategy, implemented in Figure 6 using a range of different initial conditions, the system chooses whether it is preferable to approach the destination in reverse, rather than forward translational speed. The decision is based on which side of the y axis it starts on, and how close to the destination the initial position is. Note that the brief period during which

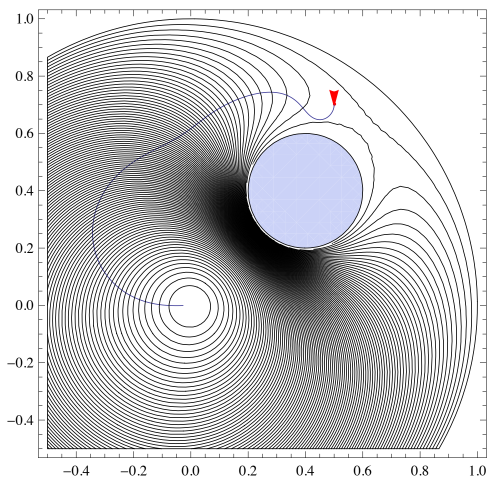

Fig. 4 Simulated path of (1) under (5). The system starts at $x = 0.5$, $y = 0.7$ at $t = 0$, with orientation $\theta = -\frac{\pi}{2}$, and converges to a neighborhood of the origin. The initial configuration is marked by an arrow having the same direction as the unicycle.

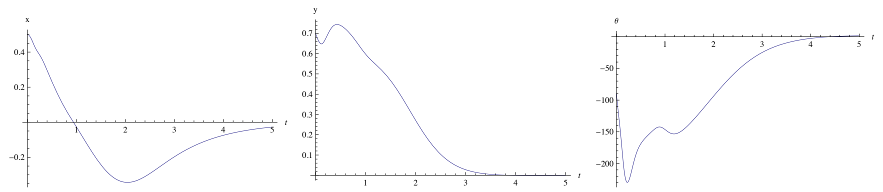

(a) x over time. (b) y over time. (c) Orientation θ over time.

Fig. 5 Simulated time evolution for the three configuration variables of the unicycle under control (5), starting from $(0.5, 0.7, -\frac{\pi}{2})$ and over a period of five (simulation) seconds.

the robot enters the shaded region is not sufficient to activate the guard and trigger its speed switching. We also note that neither in our simulations, nor in our experiments did the system overshoot,[5] and for a $\delta \geq 0.5$ seconds the time it spent inside the neighborhood was not enough to trigger any on-line speed switches.

6 Experimental Results

We implemented the navigation strategy (5) on a small four-wheel drive mobile robot with skid steering, manufactured by Coroware™ (Figure 1). The robot was confined to move in a rectangular area inside our laboratory (part of the boundary is marked with red tape in Figure 7) which can be mathematically modeled as an ellipsoid of the form $\beta_0(q) = 1 - \left(\frac{x-x_c}{a}\right)^{2n} + \left(\frac{y-y_c}{b}\right)^{2n}$ for $a, b > 0$ and $n \in \mathbb{N}_+$, and can then be diffeomorphically transformed into

[5] We hypothesize that this was because of the low speed close to the origin.

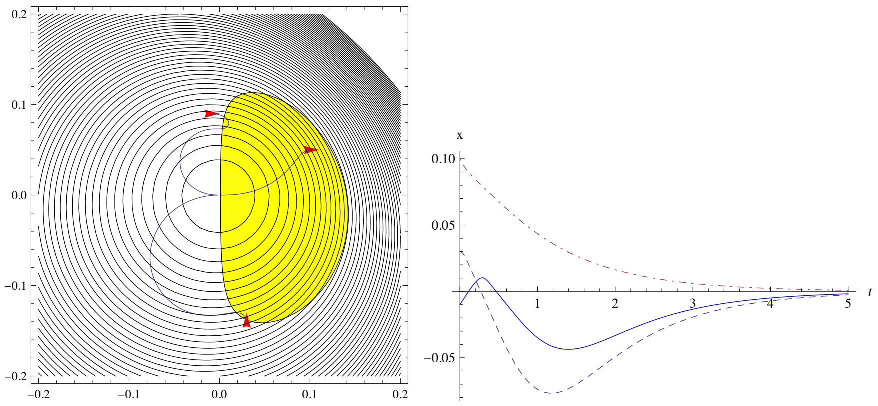

(a) Robot paths. (b) x over time.

Fig. 6 Simulated robot paths using (6) and the hybrid dynamics of Definition 1, from different initial conditions (Figure 6(a)). The shaded region in Figure 6(a) indicates the neighborhood of the origin from where initial conditions cause the system to start with a reverse speed. Figure 6(b) shows the evolution of the x coordinate in each of the cases depicted in Figure 6(a), indicating that there was not enough time to trigger a speed switch in the cases where the system entered the shaded region having forward speed.

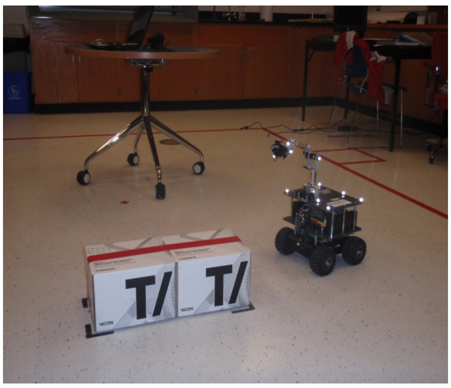

Fig. 7 The mobile robot used in the experiment. It is a four wheel drive vehicle with skid steering, and it is being localized using a basic motion capture system from Vicon™ with eight cameras mounted on the surrounding walls. The rolling table seen in the background plays the role of the circular obstacle in our experiments.

a disk like the one depicted in Figure 4 using the translated scaling mapping of [42]. The robot's position and orientation is obtained using a Vicon™ motion capture system with eight cameras which track a pattern of reflective markers attached to the vehicle; these markers can be seen as the shiny dots in Figure 7.

The time profile of the position and orientation of the robot is recorded on the robot's on-board computer on-line, as position and orientation feedback is provided by the Vicon™ system directly to the robot over wi-fi. The controller is implemented in C++ and executed on the robot's onboard Atom 1.6GHz processor.

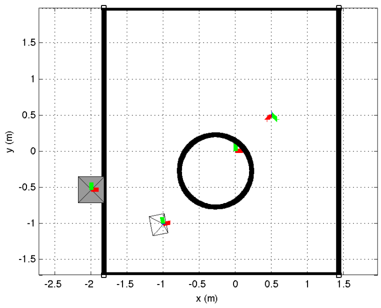

(a) Initial configuration.

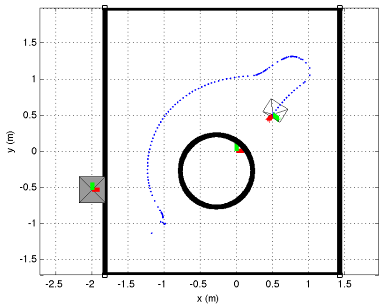

(b) Path and final configuration.

Fig. 8 A graphical depiction of the path that the robot followed during the experiment. The workspace is outlined as a rectangle, the round table is shown as a disk and is treated as an obstacle. Figure 8(a) shows the initial configuration for the robot, where one can also see the desired configuration depicted as a frame attached at location with coordinates $(0.5, 0.5)$. Figure 8(b) marks with the dotted line the path that the robot followed from its initial to the desired configuration, and the dots in the path are coordinates provided by the Vicon$^{\text{TM}}$ system, separated by a time interval of one second.

For the experimental scenario, the origin of the fixed coordinate system falls within the circular obstacle region occupied by the table (the frame is marked with a small L-shape pointer at location $(0, 0)$ m in Figure 8). The desired robot position is a point with coordinates $(0.5, 0.5)$ m, and the desired orientation is $225.5°$ or equivalently, $-134.5°$. The desired configuration is also marked with a small L pointer, rotated by $-134.5°$. The robot is randomly placed "behind" the circular obstacle, in a region where the destination is not in the direct line-of-sight. The initial configuration was measured by the Vicon$^{\text{TM}}$ system to be at $(x_0, y_0, \theta_0) = (-1.0018, -1.0158, 11°)$, and the robot in its initial position is shown in Figure 8(a) as a rectangle with a thin outline and a body-fixed reference frame attached to its front side. Figure 8(b) shows the trail of the robot on its way to its desired configuration, and its configuration at the end of a 144 second time period. The intermediate points along the path are marked based on the Vicon$^{\text{TM}}$ data, which are shown in detail for the position and orientation in Figure 9. The initial and desired configurations were selected so that they can present navigational and computational challenges: desired orientation nonzero and in $180°$ degree difference compared to initial, and desired position on the opposite side of an obstacle. In the same workspace configuration we have not observed any combination of initial and final conditions that required significantly more challenging maneuvering on the part of the robot. Having said that, it needs to be acknowledged that the approach has not yet been tested in more complex obstacle environments involving non-convex obstacles—rectangular shapes can still be handled effectively.

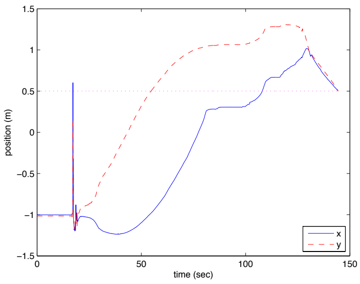

(a) Planar position (x, y).

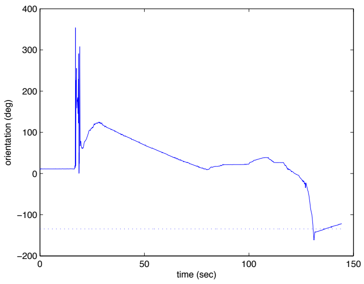

(b) Orientation.

Fig. 9 The time profiles of the configuration of the robot during the experiment, as recorded by the VICON$^{\text{TM}}$ system. The dotted horizontal lines mark the desired position and orientation. The spikes recorded at initial time are spurious local position estimates by the motion capture system.

Two observations are made with reference to Figure 9. The first concerns the spikes shown at initial time; these are spurious VICON$^{\text{TM}}$ estimates of the robot's position and orientation, which are most likely caused by reflections from the (relatively shiny) floor in the neighborhood of the initial configuration. Such outliers can infrequently also occur due to motion capture calibration errors or temporary loss of line of sight to the markers by a number of cameras. These effects are random in nature and do not necessarily repeat in subsequent tests with the same initial conditions and parameters.

A second observation is with regards to the final position reached. Although the desired position is reached quite accurately (Figure 9(a)), the orientation exhibits a small error at the end of the 144 second run, which is of the order of $12°$. There can be multiple sources for the residual orientation error, one of them being the skidding mechanism that the robot uses in order to turn, which is inherently inaccurate. A component of this residual orientation error, however, is also systemic: the orientation that is given to the robot as a reference when close to the destination is essentially that of a tangent to a circle that passes through the current position and the origin and is tangent to the x-axis at zero. Although this desired orientation converges to zero along the circular arc as the latter is traversed toward the origin, small errors in the y coordinate result to orientation references significantly different from zero —this phenomenon is related to the fact that the destination is not Lyapunov stable. In short, a control law of the form (5) makes the convergence of the orientation to be sensitive to that of position.

An obvious way to try to alleviate the residual orientation errors caused by this dependence is to have the robot converge to the x axis of the desired frame as early as possible, and then follow it toward the destination. Dilations can be used to “bend” the integral curves of the dipolar field around the destination to this effect, if deemed necessary.

For our implementation, and possibly due to the small translational speed in the neighborhood of the destination, we did not observe any overshoot, and thus control law (5) was adequate for our tests.

7 Conclusions

For nonholonomic mobile robots moving on the plane, this paper offers a new method to combine navigation function based collision avoidance and motion planning with nonholonomic control (both position and orientation). The distinguishing feature of new method compared to existing solutions is that it allows the simultaneous convergence of both position and orientation while reducing the need for on-line switching between different control laws, which can cause chattering phenomena. The convergence properties of the method can be shown analytically and the suitability for implementation is demonstrated through experiments with a differential-drive, skid steering mobile robot.

The implementation also reveals that the method may be sensitive to implementation limitations that may cause the vehicle to overshoot its desired posture, forcing it to move away from the desired position before approaching it again; this behavior is consistent with the nature of the nonholonomic constraints that the system is subject to. Lastly, the convergence speed of the different state variables may not be uniform; the proposed approach tends to stabilize position faster and more accurately than vehicle orientation.

Acknowledgements This work is partially supported by ARL MAST CTA #W911NF-08-2-0004

References

1. Astolfi, A.: Discontinuous control of nonholonomic systems. Systems & Control Letters **27**, 37–45 (1996)
2. Barraquand, J., Langlois, B., Latombe, J.C.: Numerical potential fields techniques for robot path planning. IEEE Transactions on Systems, Man and Cybernetics **22**, 224–241 (1992)
3. Bloch, A.M., Drakunov, S.V., Kinyon, M.K.: Stabilization of nonholonomic systems using isospectral flows. SIAM Journal on Control and Optimization **38**(3), 855 – 874 (2000)
4. Brockett, R.: Asymptotic stability and feedback stabilization, pp. 181–191. Differential Geometric Control Theory. Birkhauser, Boston (1983)
5. Brockett, R.W.: Asymptotic stability and feedback stabilization. In: R. Brockett, R. Millman, H. Sussmann (eds.) Differential Geometric Control Theory, pp. 181–191. Birkhauser, Boston (1983)
6. Chen, J., Dixon, W.E., Dawson, D.M., Galluzzo, T.: Navigation and control of a wheeled mobile robot. In: Proceedings of the IEEE/ASME Conference on Advanced Intelligent Mechatronics, pp. 1145–1150. Monteray CA (2005)
7. Choset, H., Lynch, K.M., Hutchinson, S., Kantor, G., Burgard, W., Kavraki, L.E., Thrun, S.: Principles of Robot Motion: Theory, Algorithms, and Implementations. MIT Press, Boston (2005)

8. Clarke, F.H., Ledyaev, Y.S., Sontag, E.D., Subbotin, A.I.: Asymptotic controllability implies feedback stabilization. IEEE Transactions on Automatic Control **42**(10), 1397–1407 (1997)
9. Conner, D.C., Choset, H., Rizzi, A.A.: Flow-through policies for hybrid controller synthesis applied to fully actuated systems. IEEE Transactions on Robotics **25**(1), 136–146 (2009)
10. Connolly, C., Burns, J., Weis, R.: Path planning using laplace's equation. In: Proceedings of IEEE Conference on Robotics and Automation, pp. 2102–2106. Cincinnati, OH (1990)
11. Coron, J.M., Rosier, L.: A relation between continuous time-varying and discontinuous feedback stabilization. Journal of Mathematical Systems, Estimation and Control **4**(1), 67–84 (1994)
12. D. Tilbury, R.M., Sastry, S.: Trajectory generation for the n-trailer problem using Goursat normal forms. IEEE Transactions on Robotics and Automation **40**, 802–819 (1995)
13. Dimarogonas, D.V., Kyriakopoulos, K.J.: On the state agreement problem for multiple unicycles with varying communication links. In: Proceedings of the 45th Conference on Decision and Control, pp. 4283–4288 (2006)
14. Ferrara, A., Rubagotti, M.: Second-order sliding-mode control of a mobile robot based on a harmonic potential field. IET Control Theory & Applications **2**(9), 807–818 (2008)
15. Filippov, A.: Differential Equations with Discontinuous Righthand Sides. Kluwer Academic Publishers (1988)
16. Guldner, J., Utkin, V.: Sliding mode control for an obstacle avoidance strategy based on an harmonic potential field. In: Proceedings of the 32nd IEEE Conference on Decision and Control, pp. 424–429 (1993)
17. Guldner, J., Utkin, V.: Sliding mode control for gradient tracking and robot navigation using artificial potential fields. IEEE Transactions on Robotics and Automation **11**(2), 247–254 (1995)
18. Kallem, V., Komoroski, A.T., Kumar, V.: Sequential composition for navigating a nonholonomic system in the presense of obstacles. IEEE Transactions on Robotics **27**(6), 1152–1159 (2011)
19. Khalil, H.K.: Nonlinear Systems. Second Edition. Prentice-Hall Inc. (1996)
20. Khatib, O.: Real-time obstacle avoidance for manipulators and mobile robots. International Journal of Robotic Research **5**(1), 90–98 (Spring, 1986)
21. Kim, J., Khosla, P.: Real-time obstacle avoidance using harmonic potential functions. IEEE Transactions on Robotics and Automation **8**(3), 338–349 (1992)
22. Koditschek, D.E., Rimon, E.: Robot navigation functions on manifolds with boundary. Advances in Applied Mathematics **11**, 412–442 (1990)
23. Koksal, M., Gazi, V., Fidan, B., Ordonez, R.: Tracking a maneuvering target with a non-holonomic agent using artificial potentials and sliding mode control. In: 16th Mediterranean Conference on Control and Automation, pp. 1174–1179 (2008)
24. Krogh, B.: A generalized potential field approach to obstacle avoidance control. In: Proc. of SME Conference on Robotics Research. Bethlehem, PA (1984)
25. Kyriakopoulos, K.J., Kakambouras, P., Krikelis, N.J.: Navigation of nonholonomic vehicles in complex environments with potential fields and tracking. In: Proceedings of the 1996 IEEE International Conference on Robotics and Automation, pp. 3389–3394 (1996)
26. Lafferriere, G., Sontag, E.: Remarks on control lyapunov functions for discontinuous stabilizing feedback. In: Proceedings of the 32^{nd} IEEE Int. Conf. on Decision and Control, pp. 2398–2403. San Antonio, TX (1993)
27. Lafferriere, G., Sussmann, H.: A differential geometric approach to motion planning. In: Z. Li, J. Canny (eds.) Nonholonomic Motion Planning, pp. 235–270. Kluwer Academic Publishers (1993)
28. Lamiraux, F., Bonnafous, D., Lefebvre, O.: Reactive path deformation for nonholonomic mobile robots. IEEE Transactions on Robotics **20**(6), 967–977 (2004)
29. Laumond, J.P., Jacobs, P.E., Taïx, M., Murray, R.M.: A motion planner for nonholonomic mobile robots. IEEE Transactions on Robotics and Automation **10**(5), 577–592 (1994)

30. Liu, Z., Jing, R., Ding, X., Li, J.: Trajectory tracking control of wheeled mobile robots based on the artificial potential field. In: Proceedings of the Fourth International Conference on Natural Computation, vol. 7, pp. 382–387 (2008)
31. Loizou, S.G., Kyriakopoulos, K.J.: Centralized feedback stabilization of multiple nonholonomic agents under input constraints. In: 5th IFAC Symposium on Intelligent Autonomous Vehicles (2004)
32. Loizou, S.G., Tanner, H.G., Kumar, V., Kyriakopoulos, K.: Closed loop motion planning and control for mobile robots in uncertain environment. In: 42th IEEE Conference on Decision and Control, pp. 2010–2015. Maui, Hawaii (2003)
33. Lopes, G.A., Koditschek, D.E.: Navigation functions for dynamical, nonholonomically constrained mechanical systems. In: S. Kawamura, M. Svinin (eds.) Advances in Robot Control; From Everyday Physics to Human-Like Movements, pp. 135–156. Springer, New York (2006)
34. Lopes, G.A.D., Koditschek, D.E.: Visual servoing for nonholonomically constrained three degree of freedom kinematic systems. The International Journal of Robotics Research **26**(7), 715–736 (2007)
35. Luca, A.D., Oriolo, G., Samson, C.: Feedback control of a nonholonomic car-like robot. In: J.P. Laumond (ed.) Robot Motion Planning and Control (Lecture Notes in Control and Information Sciences), vol. 229, pp. 171–253. Springer-Verlag (1998)
36. Masoud, A.: A harmonic potential field approach for navigating a rigid, nonholonomic robot in a cluttered environment. In: Proceedings of the IEEE International Conference on Robotics and Automation, pp. 3993–3999 (2009)
37. Murray, R., Sastry, S.: Nonholonomic motion planning : Steering using sinusoids. IEEE Transactions on Automatic Control pp. 700–716 (1993)
38. Oriolo, G., Luca, A.D., Vantittelli, M.: WMR control via dynamic feedback linearization: design, implementation, and experimental validation. IEEE Transactions on Control Systems Technology **10**(6), 835–852 (2002)
39. Panagou, D., Tanner, H.G., Kyriakopoulos, K.J.: Dipole-like fields for stabilization of systems with Pfaffian constraints. In: Proc. of the 2010 IEEE International Conference on Robotics and Automation, pp. 4499–4504. Anchorage, Alaska (2010)
40. Pathak, K., Agrawal, S.: Planning and control of a nonholonomic unicycle using ring shaped local potential fields. In: Proceedings of the American Control Conference, vol. 3, pp. 2368–2373 (2004)
41. Pomet, J.P.: Explicit design of time-varying stabilizing control laws for a class of controllable systems without drift. Systems & Control Letters **18**, 147–158 (1992)
42. Rimon, E., Koditschek, D.: Exact robot navigation using artificial potential functions. IEEE Transactions on Robotics and Automation **8**(5), 501–518 (1992)
43. Roussos, G., Dimarogonas, D.V., Kyriakopoulos, K.J.: 3D navigation and collision avoidance for nonholonomic aircraft-like vehicles. International Journal of Adaptive Control and Signal Processing **24**(10), 900–920 (2010)
44. Samson, C.: Time-varying feedback stabilization of a car-like wheeled mobile robot. International Journal of Robotics Research **12**(1), 55–66 (1993)
45. Sekhavat, S., Laumond, J.P.: Topological property for collision-free nonholonomic motion planning: The case of sinusoidal inputs for chained form systems. IEEE Transactions on Robotics and Automation **14**(5), 671–680 (1998)
46. Sekhavat, S., Švestka, P., Laumond, J.P., Overmars, M.H.: Multi-level path planning for nonholonomic robots using semi-holonomic subsystems. International Journal of Robotics Research **17**(8), 840–857 (1998)
47. Singh, L., Stephanou, H., Wen, J.: Real-time robot motion control with circulatory fields. In: Proc. of IEEE Conference on Robotics and Automation, pp. 2737–2742. Minneapolis, MN (1996)
48. Tanner, H., Kyriakopoulos, K.: Nonholonomic motion planning for mobile manipulators. In: Proc. of the 2000 IEEE International Conference on Robotics and Automation, pp. 1233–1238. San Francisco (2000)
49. Tanner, H.G., Loizou, S.G., Kyriakopoulos, K.J.: Nonholonomic stabilization with collision avoidance for mobile robots. In: Proc. of the 2001 IEEE/RSJ International Conference on Intelligent Robots and Systems, pp. 1220–1225. Maui, Hawaii, USA (2001)

50. Tanner, H.G., Loizou, S.G., Kyriakopoulos, K.J.: Nonholonomic navigation and control of cooperating mobile manipulators. IEEE Transactions on Robotics and Automation **19**(1), 53–64 (2003)
51. Urakubo, T., Okuma, K., Tada, Y.: Feedback control of a two wheeled mobile robot with obstacle avoidance using potential functions. In: Proceedings of the 2004 IEEE/RSJ International Conference on Intelligent Robots and Systems, vol. 3, pp. 2428–2433 (2004)
52. Utkin, V., Drakunov, S., Hashimoto, H., Harashima, F.: Robot path obstacle avoidance control via sliding mode approach. In: IEEE/RSJ International Conference on Intelligent Robots and Systems, pp. 1287–1290 (1991)
53. Canudas de Wit, C., Sordalen, O.: Exponential stabilization of mobile robots with nonholonomic constraints. IEEE Transactions on Automatic Control **13**(11), 1791–1797 (1992)

A Transformed Vector Field Properties

Lemma 1 *All integral manifolds of $-\Gamma\ (x,y)^\mathsf{T}$ are closed curves that contain the origin, and the latter is the only singular point of the vector field. Furthermore, as the integral curves approach the origin, the direction of the tangent vector converges to zero.*

Proof Let us consider the field $-\Gamma\ (x,y)^\mathsf{T}$ and $(x^2-y^2, 2xy)^\mathsf{T}$. The cross product of the two vector fields when embedded in $\mathbb{R}^3$ produces a third, which has as its third component the expression $-y\cos(\arctan2\,(y,x)) + x\sin(\arctan2\,(y,x)) \equiv 0$. This means that at any point $(x,y,0)$, the directions of vector fields $-\Gamma\ (x,y)^\mathsf{T}$ and $(x^2-y^2, 2xy)^\mathsf{T}$, coincide. The latter field, $(x^2-y^2, 2xy)^\mathsf{T}$, is known in literature [26] to produce closed orbits which are circles tangent to each other at the origin.

The fact that the origin is the only singular point is obvious since Γ is nonsingular, and $-(x,y)$ has the origin as a stable node. Therefore, as the flow of any one of these vector fields moves along these orbits, it will eventually encounter the origin. On the other hand, the argument that the direction of the vector fields, given by $2\arctan2\,(y,x)$ converges to zero as the integral curve approaches the origin is found in [53].

Lemma 2 *The field $-\Gamma\ \nabla\varphi$ maintains the collision avoidance properties of the field $-\nabla\varphi$ that has been generated by the navigation function φ.*

Proof On the boundary of the free workspace, $\partial\bigcup_{i=1}^m \mathcal{O}_i(q) = 1$ and therefore $s_d(q) = 0$. When this happens, $z = \pi\ \mathrm{sign}(y) = \pm\pi$ which means that $\Gamma(z) = I_2$, where I_2 is the identity matrix on $\mathbb{R}^2$. If φ is a navigation function, then its negated gradient points away from $\partial\bigcup_{i=1}^m \mathcal{O}_i$. On the workspace boundary, the transformed field coincides with the potential field of the navigation function, and thus inherits its collision avoidance properties.

Lemma 3 *Transformation Γ introduces stationary points with empty attraction regions.*

Proof The Γ function exhibits discontinuity on the $y = 0$ line, because of the sign function it involves. The positive x semi-axis is particularly problematic, because this is where the transformed field $-\Gamma\ \nabla\varphi$ will be directly opposed that of $-\nabla\varphi$ (Figure 3); somewhere on this line the vector field will have to reverse direction, and this is exactly where the stationary point appears.

For any small neighborhood of $(x,y) = (0,0)$ and any $\epsilon > 0$, there are points in this neighborhood for which there is a sufficiently small a such that $s_d(x,y) < \epsilon$. This essentially ensures that the transition, or "blending," of the dipole field of Figure 3(b) with that of $-\nabla\varphi$ occurs within that neighborhood. Note that as $(x,y) \to (0,0)$, since $\prod_{i=1}^m \beta_i$ converges to a constant and $\gamma(x,y) \to 0$, we have $\varphi(x,y) \propto \|q\|^2$. Naturally, $\langle -\nabla\varphi, -q\rangle > 0$ there, and locally, the negated gradient field of φ resembles that of the stable node shown in Figure 3(a).

Along the x-axis where $y = 0$, $-q$ is tangent to the x-axis and along each side of the axis the vector field of $-q$ points toward the axis. In the same area, where y is very small and x is positive, $\Gamma(q)$ rotates $-q$ by more than $\frac{\pi}{2}$, so that $\langle \Gamma(q)(-q), -q\rangle < 0$. What this implies is that the Filippov solutions [15] of $-\Gamma\ \nabla\varphi$ that start from the discontinuity line when $x > 0$ diverge from it. In contrast, the Filippov solutions that start at $y = 0$ when $x < 0$ form a sliding mode and "slide" along the axis as they approach the origin—these are not problematic because they converge with the desired orientation. Thus, along the discontinuity surface the only sliding motion that exists converges to the origin, whereas no solution converging to the stationary point at the positive x semi-axis exists.

Lemma 4 *All integral curves of $-\Gamma(q)\ \nabla\varphi(q)$ converge to $q = 0$ asymptotically along the negative x axis, and their common derivative at $q = 0$ is aligned with the x axis.*

Proof Trajectories are bounded in a compact set $\overline{\mathcal{W} \setminus \bigcup_{i=1}^{m} \mathcal{O}_i}$, (the bar denotes closure) so there is a limit set inside the compact set where the trajectories converge. The critical points of $-\nabla\varphi$ other than $q = 0$ do not change nature under the transformation, because Γ is continuous around any one of these critical points, and φ is Morse. Thus all critical points other than the destination $q = 0$ remain unstable, with an attraction region of measure zero. Unless there are additional attractors, the origin must be the only attractive component of the limit set.

In principle, the transformation induced by Γ may introduce a limit cycle. For a sufficiently small a, Γ is bound to apply only around $q = 0$, so if there is a limit cycle the equilibrium encircled must be $q = 0$. This implies that hypothetical limit cycle must intersect with the x-axis. However, the proof of Lemma 3 states that Γ makes the positive x-axis around the origin, repulsive. Therefore, it is not possible for trajectories to cross it on their way to the hypothetical attractive limit cycle. By contradiction, the possibility of limit cycles existing around the origin is excluded, leaving the origin as the only attractive component of the positive limit set in $\mathcal{W} \setminus \bigcup_{i=1}^{m} \mathcal{O}_i$.

To see why the integral curves of the vector field $F(q)$ near the origin (Figure 3(b)) approach $q = 0$ with zero slope, note first that these curves cannot reach the origin from the right half plane; this is because the positive x-axis is rendered repulsive. On the left half plane, near the origin and close to the x-axis, $\Gamma(q)$ converges to the identity matrix; along the y-axis the $-\Gamma\ \nabla\varphi(q)$ tends to $(\pm y, 0)^\mathsf{T}$, with the sign depending on the side of the x axis the limit is evaluated on. The only possible direction of approach to the origin for the integral curves of $-\Gamma\ \nabla\varphi(q)$ is along the negative x-axis, which suggests that the slope of the vector field $-\Gamma\ \nabla\varphi$ needs to tend to zero as $x \to 0^-$.